ELSEVIER

Journal of Nuclear Materials 290–293 (2001) 1160–1164

journal of nuclear materials

www.elsevier.nl/locate/jnucmat

ICRF wall conditioning experiments in the W7-AS stellarator

R. Brakel *, D. Hartmann, P. Grigull, W7-AS Team

Max-Planck-Institut für Plasmaphysik, Euratom-Association, Boltzmannstr. 2, D-85748 Garching, Germany

Abstract

Wall conditioning by means of ICRF-produced helium discharges is shown to be applicable in the presence of a confining stellarator magnetic field. Gas breakdown and stable discharge operation are easily achieved by poloidal double strap antennas over wide ranges of ICRF power, pressure and magnetic field. Mean plasma densities up to 3×10^{18} m^{-3} have been obtained with electron temperatures of about 20 eV at the edge. In spite of the large ionization probability at such temperatures pulsed discharges in particular are suited to remove hydrogen from the vessel leading to improved density control in the following stellarator discharges. The efficiency is comparable to that of a conventional He glow discharge. Differences with the recent tokamak results are assumed to arise from the confinement properties of the stellarator field. For example, the hydrogen removal efficiency seems to increase with power density, which is reciprocal to the tokamak results.

Keywords: W7-AS; Stellarator; Wall conditioning; ICRF

1. Introduction

In superconducting fusion devices such as the forthcoming Wendelstein 7-X stellarator conventional glow discharge conditioning (GDC) cannot be applied when the magnetic field is energized. Conditioning techniques which are applicable in the presence of a strong magnetic field are therefore mandatory. The proof-of-principle of hydrogen desorption and layer deposition by ICRF (ion cyclotron range of frequency) assisted wall conditioning and coating (ICC) has recently been furnished at the Tore Supra [1,2] and TEXTOR [3,4] tokamaks and is meanwhile routinely applied at the HT-7 superconducting tokamak [5].

In view of W7-X, experiments have been started at Wendelstein 7-AS to investigate the potential of ICC in a stellarator. The main objectives were to find for ICRF discharges in helium the appropriate windows of gas pressure, ICRF power and magnetic field for breakdown and stable sustainment, to characterize the discharges, to study the hydrogen isotope removal, and to compare the effect of He-ICC and He-GDC on stellarator performance. In principle, differences in the discharge characteristics and ICC efficiency may be expected between tokamak and stellarator. The stellarator field confines charged particles, whereas the toroidal tokamak field does not due to lack of rotational transform.

2. Experimental arrangement

W7-AS is a medium-sized stellarator (major radius $R = 2$ m, minor plasma radius $a \leqslant 0.19$ m, plasma volume $V_p \leqslant 1.5$ m^3, vessel volume $V_v = 7.0$ m^3, wall area $A_w \approx 30$ m^2) equipped with graphite limiters and shieldings. The stainless steel wall is boronized periodically and the device is operated at room temperature. Usual operation is at $B = 2.5$ T on the magnetic axis. In order to achieve long pulses and to improve the duty cycle the magnetic field was operated in the ICC studies only up to $B = 1.25$ T, the pulse length ranging from steady state at $B \leqslant 0.3$ T to 5 s at 1.25 T. The rotational transform was 0.4 ($q = 2.5$).

The vessel is pumped by five turbomolecular pumps with a total effective pumping speed of $S = 2300$ l/s as measured for deuterium. A quadrupole mass spectrometer head with a mass range 1–6, being capable to

* Corresponding author. Tel.: +49-089 3299 2187; fax: +49-089 3299 2584.

E-mail address: brakel@ipp.mpg.de (R. Brakel).

0022-3115/01/$ - see front matter
PII: S0022-3115(00)00554-7

separate He and D_2, is installed for residual gas analysis at a duct which is separately pumped. Before an ICRF discharge the helium flow rate was adjusted to provide the desired gas pressure and was kept constant during the discharge. The pressure was monitored by ionization gauges at various positions in the vessel and at the position of the mass spectrometer. The ionization gauges are cross calibrated to a baratron for hydrogen, deuterium and helium.

The discharges were imaged by video cameras viewing from different toroidal positions tangentially into the torus. Electron density profiles were measured along six horizontal chords of a multichannel microwave interferometer. A movable Langmuir probe was used to determine the electron density and temperature close to the last closed magnetic surface (LCMS). The attempt to determine the energy spectra of hydrogen and deuterium CX neutrals failed due to the smallness of the respective fluxes.

3. ICRF system and breakdown conditions

ICRF was applied by two poloidal double strap antennas, one with a Faraday screen (A1 at 74 MHz, power up to $P_{A1} = 120$ kW), the other without (A2 at 37 MHz, power usually below $P_{A2} = 2$ kW). Both antennas were equipped with poloidal antenna limiters. Matching of the antenna impedance to the RF generator impedance was accomplished with a double stub tuner network. The net power radiated from the antenna was measured with directional couplers and has an accuracy of about 15%.

Most strikingly, breakdown was possible only with the unshielded antenna A2. Low power of $P_{A2} = 0.5$ kW was already sufficient. Even at comparatively high power, $P_{A1} = 100$ kW, breakdown could not be achieved by the shielded antenna A1. Once a discharge was ignited by A2 it could be sustained and heated by A1. The RF electric near field of the antennas parallel to the external magnetic field is thought to be responsible for the initial gas breakdown and plasma production [4]. The Faraday screen of antenna A1 greatly reduces this RF electric field, even though it was not perfectly aligned with the magnetic field lines, whereas on antenna A2 a strong electric near field exists between the current straps and the antenna limiters. Once plasma has been generated in front of antenna A2, a slow wave can be excited that transports RF power to other regions of the torus and facilitates further ionization. Then antenna A1 can also excite the slow wave. For the used magnetic fields and generator frequencies the required minimum density for slow wave propagation is of the order of 10^{13} m^{-3}.

There is a large operation window in B, p_{He} and P_{A2} for breakdown and stable sustainment of the ICRF discharges. Ramping up the magnetic field at fixed power and pressure shows that a minimum field is required for breakdown (e.g. $B = 0.08$ T at $P_{A2} = 2$ kW, $p_{He} = 3 \times 10^{-4}$ mbar). There is no lower limit for B to sustain a once ignited discharge. At $B = 0$ an RF-glow remains. At fixed field and power a minimum pressure is required for breakdown (e.g. $p_{He} = 8 \times 10^{-5}$ mbar at $B = 0.11$ T at $P_{A2} = 2$ kW). The upper pressure limit is given by the onset of arcing at the feedthroughs of the antennas ($p_{He} = 1 \times 10^{-3}$ mbar).

4. ICRF discharge parameters

Tangential video imaging confirms confinement of the ICRF plasmas in the stellarator field. Images of the ICRF discharges resemble those of standard stellarator plasmas in W7-AS. The observed poloidal structure can be explained by an emissivity which is constant on the flux surfaces and which is radially located close to (and outside of) the LCMS [6]. The topology of the images is insensitive to the magnitude of the magnetic field, its appearance only becoming more diffuse at low fields ($B < 0.1$ T). No significant asymmetry is found by viewing from different toroidal positions.

Discharges have been characterized over the range of parameters $B = 0.4$–1.25 T, $p_{He} = 3 \times 10^{-5}$–$6 \times 10^{-4}$ mbar, $P_{A1} = 7$–120 kW, $P_{A2} = 0.6$ kW. For all conditions the density profiles measured by interferometry are similar in shape, centrally peaked and symmetric. Results of a power scan at fixed field and pressure are shown in Fig. 1. The mean density $\langle n_e \rangle$ (average along central chord) strongly increases with ICRF power, moderately with the gas pressure (Fig. 2), and is nearly insensitive to the magnetic field. The highest density achieved is $\langle n_e \rangle = 2.8 \times 10^{18}$ m^{-3}. The Langmuir probe data included in Fig. 2 were obtained at an effective plasma radius of 0.175 m close to but inside the LCMS-radius of $a = 0.192$ m. The edge density derived from the probe is typically a factor of 10 smaller than the mean density and shows a similar power scaling. At the LCMS the degree of ionization $\alpha = n_e/(n_e + n_{He})$ ranges from $\alpha = 3 \times 10^{-3}$ at low power/high pressure to $\alpha = 0.2$ at high power/low pressure. The electron temperature close to the LCMS is between 20 and 25 eV and shows no strong variation with ICRF power and gas pressure. At $T_e = 20$ eV the rate coefficients for electron impact ionization are 4×10^{-15} m^3/s for He and 2×10^{-15} m^3/s for H_2 resulting in ionization times $\tau_i < 20$ ms at the LCMS. It has to be noted that possible potential fluctuations due to the RF-field may perturb the probe characteristic such that the electron temperature and density derived by the standard probe theory have to be considered as the upper and lower limits, respectively [7].

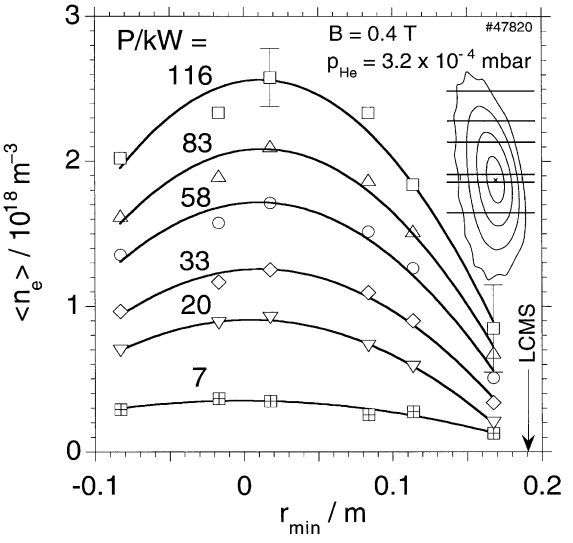

Fig. 1. Profiles of the line-averaged density at different ICRF powers P_{A1}. r_{min} is the effective radius of the flux surfaces to which the viewing chords of the interferometer (see insert) are tangential.

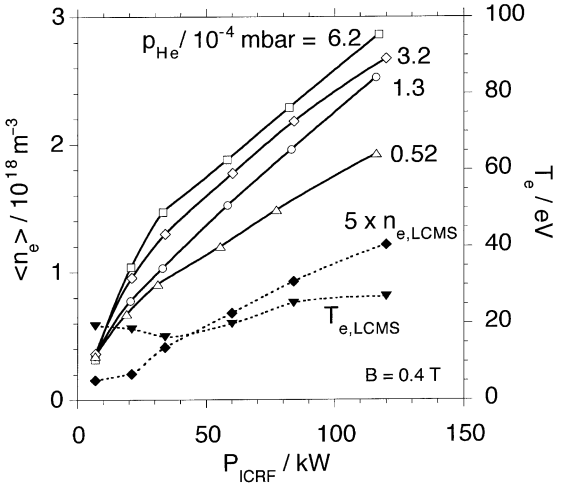

Fig. 2. Dependence of the mean density on ICRF power for different gas pressures. Density and temperature at the LCMS for $p = 3.2 \times 10^{-4}$ mbar.

5. Wall desorption

ICC desorption experiments have been performed alternate with normal stellarator discharges which were fuelled by hydrogen and heated by ECRH and hydrogen neutral beam injection. The experiments were preceded by about 600 W7-AS shots with deuterium fuelling and the wall was boronized using B_2D_6 400 shots before. Therefore all hydrogen isotopes are incorporated in the plasma facing surfaces. Fig. 3 shows the response of the deuterium partial pressure p_{D_2} to different ICRF heating scenarios with powers $P_{A1} = 12$ kW and $P_{A2} = 0.6$ kW. The total pressure in the vessel was $p = 3.2 \times 10^{-4}$ mbar before the discharge and the constant He-flow was turned off at the end of the heating phase. In case (a) both antennas were operated continuously (cw), in case (b) A2 was operated continuously and A1 pulsed (10 s on/10 s off), and in case (c) both antennas were synchronously pulsed. p_{D_2} decreases whenever ICRF is on, i.e. deuterium is effectively pumped by the plasma and after redeposition by the wall even in phases with low heating power (case (b), when A2 is off). This can be understood by the fact that the ionization time $\tau_i < 20$ ms is much smaller than the pumping time $\tau_{pump} = V_v/S = 3$ s. Wall desorption and outgassing of hydrogen isotopes become evident by the strong increase in the respective partial pressures whenever ICRF is switched off. This behaviour is in contrast to both in tokamak ICC discharges [2] and in a He glow discharge, where the hydrogen partial pressures at a pump duct increase immediately after breakdown, i.e. there is an effective removal already during the discharge.

In Fig. 4 both ICRF antennas are operated in a pulsed mode (15 s on/15 s off) with a pulse-to-pulse increase of P_{A1} from 0 to 50 kW and $P_{A2} = 0.6$ kW for each pulse. Here, the total pressure was $p = 1.3 \times 10^{-4}$ mbar before the discharge and the He-flow was kept constant also during the pump-out phase. The modulation depth of the partial pressure is much higher for deuterium than for helium; this is assumed to be due to a much higher sticking probability of wall-redeposited deuterium. Absolute values of p_{D_2} and p_{He} have been obtained by scaling the uncalibrated mass spectrometer traces such that the sum of the respective partial pressures fits the pressure p_{IG2} measured by the ionization

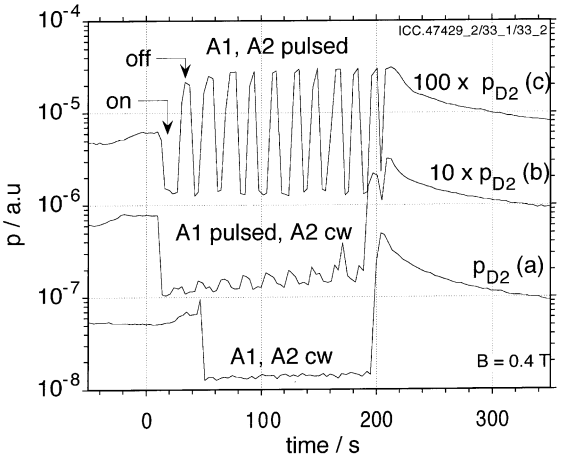

Fig. 3. D_2 partial pressure for three heating scenarios with $P_{A1} = 12$ kW, $P_{A2} = 0.6$ kW ($p = 3.2 \times 10^{-4}$ mbar).

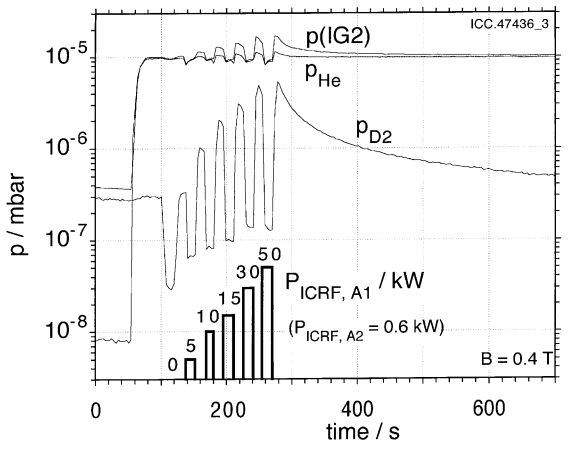

Fig. 4. Pressure at the mass spectrometer (ionization gauge, absolute pressure in the vessel: $p = 1.3 \times 10^{-4}$ mbar), partial pressures of He and D_2, and power of antenna A1 for a sequence of ICRF-pulses (15 s on/15 s off).

gauge at the mass spectrometer. With this scaling the deuterium pressure p_{D_2} represents the total amount of the different hydrogen species. The amount of hydrogen isotopes removed from the vessel by this discharge cycle is estimated by the time integral of the increase of p_{D_2} above its initial value. Along with the effective pumping speed, the ratio of pressure in the vessel to pressure at the mass spectrometer (2.0), and the measured ionization gauge correction factor (3 for D_2), this yields an amount of gas removed from the vessel of 6 mbar l equivalent to 1.5×10^{20} molecules.

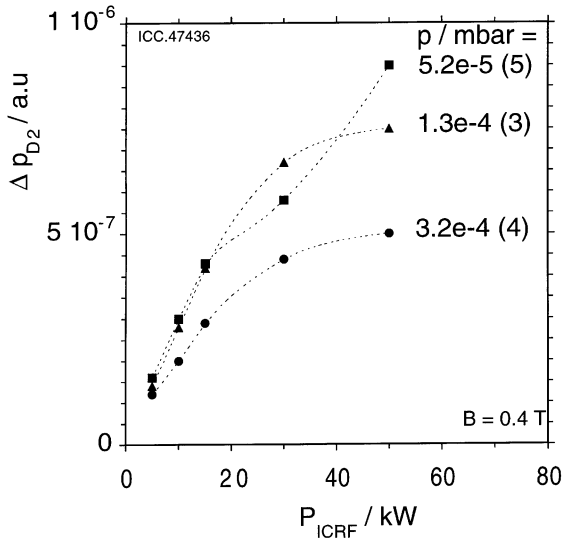

Fig. 5. Increase of D_2 partial pressure in response to 15 s ICRF pulses versus power for different He pressures.

The increase Δp_{D_2} of deuterium pressure after each ICRF pulse in Fig. 4 is taken as a relative measure for the efficiency of D_2-removal. (Correcting for the amount of gas not yet pumped from the preceding pulses basically changes only the absolute scale of Δp_{D_2}). Fig. 5 summarizes the results of three consecutive discharge cycles like that in Fig. 4 at different helium pressures. The curves are labelled by the helium pressure and, in brackets, by the number within the sequence of cycles. At constant pressure the removal efficiency increases with power, tending to saturate at 50 kW. It is furthermore indicated that the removal efficiency decreases with the He-pressure. This dependence is reciprocal to the Tore Supra and TEXTOR results, where the conditioning efficiency is found to decrease with the power density, P_{ICRF}/p_{He} [1,4].

He-ICC significantly improved density control in stellarator discharges. For example, after conditioning (five cycles like those in Fig. 4 at p = 3.2, 6.2, 1.3, 3.2 and 0.52×10^{-4} mbar, total time of ICRF application 7.5 min) the amount of injected hydrogen atoms required to ramp up an ECRF heated plasma to a mean density flat top of 6×10^{19} m^{-3} (corresponding to 9×10^{19} electrons and hydrogen ions, respectively) increased from 2.4×10^{20} before ICC to 3.8×10^{20} later, the difference being attributed to enhanced wall pumping. For comparison, the amount of hydrogen removed from the wall by ICC is estimated to be about 1.5×10^{21} atoms. Furthermore, density control in NBI discharges that had been lost after high density shots could be recovered after ICC. These beneficial effects on stellarator performance are comparable with that of 10 min He-GDC.

6. Discussion

Wall conditioning by means of ICRF produced helium discharges has been shown to be applicable in a stellarator. With an unshielded ICRF antenna breakdown is easily achieved at very low power over a wide range of gas pressures and the discharges can be sustained and heated by a shielded antenna. The discharge parameters are rather insensitive to the magnetic field value. Wall desorption and removal of hydrogen are evident from mass spectroscopy and the effect of He-ICC on stellarator performance (improved density control) is comparable to that achieved by He-GDC.

Compared to tokamaks, ICC in W7-AS shows some significant differences. (i) At similar power density the electron temperature (about 20 eV at the LCMS) is higher at least than the values reported for Tore Supra (<10 eV). (ii) Because of the short ionization time at this temperature, pulsed ICC appears to be favourable for effective hydrogen removal as compared with continuous operation. (iii) In pulsed operation the hydrogen

removal efficiency seems to increase with the power density (the significance of this dependence has to be checked in further experiments). These differences are assumed to be due to confinement in the stellarator field which is confirmed by video imaging as well as by the strong increase of the electron density from the edge towards the centre.

References

[1] E. de la Cal, E. Gauthier, Plasma Phys. Contr. Fus. 39 (1997) 1083.
[2] E. Gauthier et al., J. Nucl. Mater. 241–243 (1997) 553.
[3] H.G. Esser et al., J. Nucl. Mater. 241–243 (1997) 861.
[4] A. Lyssoivan et al., Final Report on ITER Design Task D350.2, Ecole Royale Militaire, Brussels, 1998, Report-No. 114.
[5] Y.K. Xie, these Proceedings.
[6] J.V. Hofmann et al., Plasma Phys. Contr. Fus. 38A (1996) 193.
[7] N. Hershkovitz, in: O. Auciello, D.L. Flamm (Eds.), Plasma Diagnostics, vol. 1, Academic Press, Boston, 1989, p. 113.